Relationships of skin depths and temperatures when varying pulse repetition frequencies from 2.0-μm laser light incident on pig skin

David Schaaf
Thomas Johnson
Colorado State University
Department of Environmental and Radiological Health Sciences
1618 Campus Delivery
Fort Collins, Colorado 80523

Abstract. Human perception of 2.0-μm infrared laser irradiation has become significant in such disparate fields as law enforcement, neuroscience, and pain research. Several recent studies have found damage thresholds for single-pulse and continuous wave irradiations at this wavelength. However, the only publication using multiple-pulse irradiations was investigating the cornea rather than skin. Literature has claimed that the 2.0-μm light characteristic thermal diffusion time was as long as 300-ms. Irradiating the skin with 2.0-μm lasers to produce sensation should follow published recommendations to use pulses on the order of 10 to 100 ms, which approach the theoretical thermal diffusion time. Therefore, investigation of the heating of skin for a variety of laser pulse combinations was undertaken. Temperatures of *ex vivo* pig skin were measured at the surface and at three depths from pulse sequences of six different duty factors. Differences were found in temperature rise per unit exposure that did not follow a linear relation to duty factor. The differences can be explained by significant heat conduction during the pulses. Therefore, the common heat modeling assumption of thermal confinement during a pulse may need to be experimentally verified if the pulse approaches the theoretical thermal confinement time. [DOI: 10.1117/1.3477324]

Keywords: laser; duty factor; skin; temperature; infrared.

Paper 10029RR received Jan. 19, 2010; revised manuscript received May 4, 2010; accepted for publication Jun. 12, 2010; published online Aug. 11, 2010.

1 Introduction

The irradiation of skin by laser light has been a subject of study since shortly after the ruby laser was introduced in 1960,[1] with the first publication on rabbit and human skin in 1963.[2] From very early in the history of lasers, skin irradiation safety limits have been based on both pulsed (0.1 J/cm^2) and CW (1.0 W/cm^2) operation.[3] Current safety standards from the American National Standards Institute (ANSI) set the skin exposure limit in the infrared (IR) at $0.56 \times t^{0.25}$, in units of J cm^{-2}, where t is the exposure time between 10^{-3} and 10 s. (Ref. 4). The ANSI report is based on observed damage thresholds to the cornea of the eye, quantified in radiant exposure, H (J/cm^2) (Ref. 5). From dermatology, skin damage is described in units of temperature. Accurate temperature prediction is important because the gap between skin tolerance and injury is as narrow as 3 to 6°C, depending on duration of heating.[6–8]

The skin temperature change due to IR laser irradiation has been measured in many studies with temperature and time as predictors of skin damage.[6] Moncrief sets the threshold for irreversible damage to the basal cells of the epidermis at 44°C for extended time in minutes. For brief exposures, Moncrief gives 51°C as the limiting temperature.[7] Leach et al. had reported 47°C as the critical temperature for visible change to skin and 50 to 55°C as the threshold for permanent damage.[8]

Establishing injury thresholds from laser irradiation with very short durations often focuses on the energy and leaves temperature to calculation rather than measurement.[9] The most frequent method of skin temperature measurement during laser irradiation has been the noncontact IR camera. This type of instrument was used for single pulses of 2.0-μm laser by Chen et al.[5] Pulsed irradiation of skin with 2.94-μm laser was measured by a thermal imaging camera.[10] IR pyrometers have also been used to measure surface temperatures during laser irradiation.[11,12] Leandri et al. again demonstrated the difficulties in temperature measurement with a correlation of temperature to laser energy, but not to pulse duration.[11] Temperatures deep within tissue during and following continuous wave (CW) laser irradiation have also been measured with thermocouples.[13,14]

Tissue effects comparing different laser pulse conditions have been investigated for many purposes, including medical

Address all correspondence to T. Johnson, Colorado State University, Department of Environmental and Radiological Health Sciences, 1618 Campus Delivery, Fort Collins, CO 80523. Tel: 970-491-0563; Fax: 970-491-0623; E-mail: Thomas.E.Johnson@colostate.edu

1083-3668/2010/15(4)/045007/13/$25.00 © 2010 SPIE

Table 1 Sampling of laser pulse sequence manipulation studies.

Variable	Change	Constant	Result	Wavelength (μm)	Study
Pulse width	Reduced t_p	Equal tissue damage	Required H reduced	1.5	Ref. 15
				0.532	Ref. 16
				0.577	Ref. 17
Pulse width	Increase t_p	Equal radiant energy	No change in depth of coagulation	2.94	Ref. 18
Pulse width	Increase t_p	Equal radiant energy	Increased depth of coagulation	2.94	Ref. 19
				2.94	Ref. 20
PRF	Increase PRF	Equal radiant energy	Reduced temperature	2.09	Ref. 21
PRF	Reduce PRF	Equal radiant energy	Changed effect from ablation to coagulation	2.94	Ref. 22
PRF	Increase PRF	Equal radiant energy	Increased ablation to coagulation	2.94	Ref. 10
Number of pulses	Increase N_p	Equal radiant energy	Increased depth of injury	10.6	Ref. 23

uses and injury investigation. Different results have been found when one or more of the following parameters have been varied: pulse repetition frequency (PRF), pulse width combinations of different widths, different spacing (i.e., not a repetitive frequency), or sequences with different power per pulse. Pulse sequence optimization of ErYAG lasers has been of particular interest to dermatologists to replace their CO_2 lasers.

A summary of representative studies of pulse sequence effects is given in Table 1. As seen in Table 1, pulse width can change the amount of radiant energy to produce damage in tissue or change the extent of damage. Pulse repetition frequency can change the observed temperature or type of tissue damage. Increasing the number of pulses can affect the depth of injury per pulse.

Many studies use ablation or coagulation depth as a metric for pulse sequence comparison.[10,20,24] For those modeling the temperature from laser pulse irradiation, the energy deposition is assumed to be an instantaneous impulse confined within the volume of deposition.[25–29] The conditions required for this assumption to be valid depend on the optical penetration in the tissue and the rate of heat flow or thermal diffusivity of the tissue.

The optical penetration depth, d, is a measure of how deep the energy fluence will travel before being absorbed. Optical penetration depth depends on the absorption and scatter of the light in the tissue and the beam width.[30,31] For absorption-dominated tissue, the optical penetration depth is $d=1/\mu_a$. For optically turbid material, the optical penetration depth is defined by Ritz et al.[31] as

$$d=[3\mu_a(\mu_a+\mu_s')]^{-1/2}, \tag{1}$$

where μ_a is the absorption coefficient, and μ_s' is the reduced scattering coefficient [$\mu_s'=\mu_s(1-g)$, with g being the anisotropy factor]. The optical zone, where the incident energy fluence has been reduced by $1/e$, in turbid media has an additional factor to account for backscattered reflections.[30]

The 2.0-μm TmYAG laser has yet to have optical absorption and scatter properties conclusively established. The diversity of published attenuation coefficients produces a wide range of optical penetration depths, as seen in Table 2.

The heating of tissue below the skin surface is complicated by the flow of heat into or out of the volume of interest during the irradiation. Therefore, models of tissue heating are simplified if they assume that the energy is deposited as an impulse with no heat flow until the pulse has terminated. The conventional criteria for neglecting heat transfer from the irradiated tissue is for the laser pulse to be significantly smaller than the thermal diffusion time,[30] τ_{diff}, also known as the thermal relaxation time, expressed by Eq. (2), where D is the thermal diffusivity of the tissue. The thermal relaxation time, τ_{diff}, is considered to confine the heat transferred within the optical penetration depth:[30]

$$\tau_{diff}=\frac{d^2}{D}. \tag{2}$$

Analytical thermal analysis of laser pulses assume no residual thermal influence of prior pulses if the pulse length is much less than the thermal relaxation time;[37] however, these analy-

Table 2 Optical penetration depth (mm), using published constants and optical zone for a beam with a $1/e^2$ radius of 3.28 mm.

μ_a (cm^{-1})	μ_s' (cm^{-1})	Optical penetration depth, δ	Optical zone, d		
			Depth	Radial	Study
Absorption					
21.76[a]		0.460	0.460	0.460	Ref. 32
28		0.357	0.357	0.357	Ref. 33
58.02[b]		0.172	0.172	0.172	Ref. 32
Turbid					
1.75	13.25	1.127	2.209	2.017	Ref. 34
48	10	0.109	0.214	0.214	Ref. 35
82	10	0.066	0.130	0.130	Ref. 36

[a]Absorption coefficient for epidermis;
[b]absorption coefficient for dermis.

ses do not address the pulse repetition frequency—that is, the time between "impulses" of energy deposited. This assumption has been applied to pulse durations up to 300 ms. (Ref. 38). Some analytic functions have been reported to fit tissue temperature changes best for short (microsecond) pulses,[39,40] while others fit best for longer pulse widths (>100 ms).[41] However, both of these solutions were evaluated for a single laser pulse rather than for a series of pulses as a whole.[40]

The skin tissue is composed of three anatomical layers, which have different optical properties. The exterior skin layer is the stratum corneum, which ranges from 10 μm to 20 μm thick, depending on anatomic site and study. Underneath is the epidermis, ranging from 30 μm to 150 μm thick. Last, the dermis has been reported to be from 981 μm to 4000 μm thick.[42] This places the optical penetration depth of 2.0-μm laser light within the dermis if absorption is dominant in skin. If skin is a turbid medium with scatter dominant, then the penetration depth is deeper into or beyond the dermis. If skin is a mildly turbid medium with both absorption and scatter, then the optical zone is close to the border between the epidermis and dermis.

Considering pulses of 2.01 μm infrared from Tm:YAG fiber lasers, the range of published values of thermal constants listed in Table 3, combined with the range of optical zones, d, found earlier in Table 2, produce thermal diffusion times that would indicate that virtually any pulse widths are thermally confined. As shown in Table 4, different combinations of constants can produce thermal diffusion times over a range of four orders of magnitude. The thermal diffusivity, D, depends on the tissue type and any vascular perfusion.

This work explores the relationship of computed and measured temperatures of 2-μm laser light incident on pig skin with varying pulse repetition frequencies and skin depths. The objective of this work is to investigate the validity of the common assumption of isolated, thermally confined pulses used in analytical temperature modeling. The variable of interest is the duty cycle of pulsed irradiations. Measurements of temperature at the surface and internal temperature at three depths beyond the optical penetration depth were evaluated for differences of heating between sequences of varying PRF, while total energy is held constant. Temperatures predicted by models that rely on the assumption of thermal confinement within a thermal relaxation time were found to have varying agreement depending on pulse cycle duty factor. Temperature rise per unit exposure was found to be different between pulse sequence duty factors at all four depths.

2 Materials and Methods

2.1 *Temperature Measurements*

Temperature measurements of six distinct pulse sequences were taken at four *ex vivo* skin depths, nominally at the surface, at 300 μm, at 400 μm, and at 650 μm. The entire skin sample and holder with thermocouple in place was centered in the beam of a 2.0-μm laser by scanning the probe through the beam on a 2-D optical stage with a micrometer (Model TXS, Melles-Griot, Albuquerque, New Mexico) in 500-μm increments first in the N–S direction and then in the E–W direction. The measurements at central axis (CAX) of the IR beam were repeated four times for each pulse sequence on each sample of pig skin. The first sequence was also repeated another four times in order to show that the skin conditions had not changed during the measurements. Three different samples of pig skin were used at each depth for a total of nine skin samples. (Surface measurements were performed concurrently.)

Temperatures were measured with two instrument systems: an infrared camera with microbolometer array for skin surface measurements and with a type T (Copper-Constantan) microthermocouple for below-surface depths. The model S65HSV thermal imaging camera (FLIR Systems, Weisbaden, Germany) detector was composed of a 320×240 array of uncooled microbolometer detectors. The sensitivity is calibrated at 0.05°C with an accuracy specification of +2°C. Image

Table 3 Thermal constants of human and pig skin.

Tissue (depth or specifier)	Conductivity κ W m^{-1} °C^{-1}	Diffusivity D m^2 s^{-1}	Density ρ g cm^{-3}	Specific heat C J kg^{-1} °C^{-1}	Year
Human					
Stratum corneum	0.235		1.5	3600	2008 (Ref. 43)
Epidermis	0.21			3600	2000 (Ref. 44)
Epidermis	0.2			2244	2006 (Ref. 32)
Epidermis	0.23		1.2	3590	2004 (Ref. 45)
Epidermis	0.235		1.190	3600	2008 (Ref. 45)
Epidermis (forearm)	0.569				1977 (Ref. 46)
Epidermis (*in vitro*)	0.209				1977 (Ref. 47)
Dermis	0.53			3800	2000 (Ref. 44)
Dermis	0.49			3663	2006 (Ref. 32)
Dermis	0.45		1.2	3300	2004 (Ref. 45)
Dermis	0.445		1.116	3680	2008 (Ref. 43)
Dermis (forearm)	0.837				1977 (Ref. 46)
Dermis (*in vitro*)	0.293				1977 (Ref. 47)
Skin	0.23–0.414				1975 (Ref. 48)
Skin	0.45	1.10×10^{-7}			1998 (Ref. 49)
Skin	0.5			4200	2002 (Ref. 50)
Skin	0.39		1.116	3200	2003 (Ref. 51)
Skin		1.30×10^{-7}			1983 (Ref. 52)
Skin	0.37		1	4180	2000 (Ref. 53)
Skin	0.53				2001 (Ref. 54)
Skin (0.26 mm)		0.4×10^{-7}			1975 (Ref. 48)
Skin (0.45 mm)		0.6×10^{-7}			1975 (Ref. 48)
Skin (0.90 mm)		0.85×10^{-7}–1.20×10^{-7}			1975 (Ref. 48)
Skin (0–2 mm)	0.376				1975 (Ref. 48)
Skin	0.56		1.07	3400	2006 (Ref. 55)
Skin (*in vitro*)	0.82×10^{-7}–1.2×10^{-7}				2000 (Ref. 56)
Skin (*in vitro*)	0.21–0.41	0.82×10^{-7}–1.2×10^{-7}			1985 (Ref. 57)
Skin (*in vitro*)	0.293		1.2	3389	1954 (Ref. 58)
Skin (*in vivo*)	0.5–2.8	0.4×10^{-7}–1.6×10^{-7}			1987 (Ref. 59)
Tissue		1.20×10^{-7}			1985 (Ref. 60)
Tissue	0.44		1.070	3500	1986 (Ref. 61)
Animal					
pig epidermis (*in vitro*)	0.209				1977 (Ref. 47)
pig skin (opaque)	0.414	0.82×10^{-7}–0.86×10^{-7}			1975 (Ref. 48)

Table 4 Thermal relaxation times, τ_{diff}, for 2.0 μm light in both depth and radial direction using published constants (s).

		Slow thermal diffusivity[a]		Fast thermal diffusivity[a]		
μ_a (cm^{-1})	μ_s' (cm^{-1})	Depth	Radial	Depth	Radial	Study
Absorption						
21.76[b]		5.28	5.28	1.32	1.32	Ref. 33
28		3.19	3.19	0.80	0.80	Ref. 30
58.02[c]		0.74	0.74	0.19	0.19	Ref. 33
Turbid						
1.75	13.25	121.90	101.70	30.5	25.4	Ref. 32
48	10	1.10	1.15	0.29	0.29	Ref. 40
82	10	0.42	0.42	0.11	0.11	Ref. 39

[a]Fast $D = 4 \times 10^{-4}$ cm^2 s^{-1} from Bowman (Ref. 48) slow $D = 1.6 \times 10^{-3}$ cm^2 s^{-1} from Chato (Ref. 57);
[b]epidermis;
[c]dermis.

sequences were collected and sent to a PC (XPS, Dell, Round Rock, Texas) at a rate of 60 Hz, giving a temporal resolution of 17 ms per data point. The images were read and analyzed using Reasercher Pro version 2.8 (FLIR Systems, Weisbaden, Germany), which offers region of interest and line profile extraction. The camera is sensitive in the spectral range of 7.5 to 13 μm. The lens has a minimum focusing distance of 0.3 m, with a quoted spatial resolution of 1.1 mrad of divergence. The thermal camera was positioned in the same location for all exposures at one meter from the skin surface, approximately 30 deg from normal to the skin in the E–W direction in order to not interfere with the beam delivery arm. The camera was calibrated by the manufacturer using NIST traceable blackbody sources.

The model HYP-0 thermocouple (Omega Engineering, Inc., Stamford, Connecticut) consisted of the thermocouple junction imbedded in the tip of a stainless steel 33-gauge hypodermic needle. The outer diameter of the needle was 200 μm. The thermocouple response was recorded using iNet software (Omega Engineering, Inc.). The iNET settings were 150 readings per second, with the noise filter set to exclude signals over 200 Hz, signal integration time set to 0.001 s, with 4000 readings collected for 26 s of monitoring. The iNet system recording was initiated by the same pulse triggering the laser via connection to the output of the HP model 33120A wave form generator (Hewlett Packard, Palo Alto, California) with a coaxial T connector. The IPG model TLR-50-2010 Tm:YAG laser (IPG Photonics, Oxford, Massachusetts) fired as the transistor-transistor Logic (TTL) signal reached its maximum of 5 V, while the iNet was set to begin collecting data at a TTL signal of 0.5 V in order to measure the initial temperature of the tissue prior to the laser pulse. Prior to each exposure session, the thermocouple–iNet system was self-tested for connectivity, with results stored to disk. The thermocouple relative accuracy and constancy was verified three times during the study by immersion into a water bath at four different temperatures, ranging from boiling to ice water. The water temperature was determined by the average reading of four Barnstead Ever-Safe N16B organic liquid filled thermometers (Thermo Scientific, Waltham, Massachusetts). The thermocouple probe was inserted in the pig skin in the N–S direction.

Direct heating of the thermocouple probe by the 2.0-μm beam rather than the surrounding tissue, considered a significant impact in several laser studies,[62–64] was judged to be negligible in this experiment for three reasons. First, the thermocouple used was considerably smaller than the one used in the Manns study. The 33-gauge needle presents a 0.21-mm diameter as opposed to their 23-gauge needle's 0.61 mm to intercept the direct beam fluence. Second, the 2.01-μm wavelength IR of the Tm:YAG laser does not penetrate to the depth of the needle, as did the 1.06- μm beam of Manns's Nd:YAG laser.[62] For example, consider the difference 1 μm of wavelength makes in the two beams' attenuation coefficient in water. From Hale and Querry, the coefficients are 69.12 cm^{-1} at 2000 nm but only 0.12 cm^{-1} at 1060-nm wavelength.[65] Using these attenuation coefficients, weighted by the water content of skin,[30,32] the 2.0-μm beam is reduced to 19% of original intensity by Beer's law at the 0.3-mm depth of the probe. In contrast, the Nd:YAG beam in the Manns study would still be at 95% at the 5-mm distance to their closest thermocouple. Last, the graphs of skin temperature rise during the laser pulse recorded with this thermocouple did not exhibit the instantaneous temperature jump that has been claimed to be the indication of direct thermocouple absorption of laser beam energy.[63,64]

2.2 *Skin Samples*

Pig skin (Sus Scrofa Domestica) was obtained via an agreement with the professional veterinary program at Colorado State University. Approval to utilize tissue samples from these

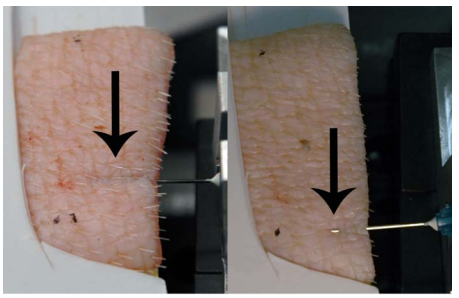

Fig. 1 Needle insertion into pig skin: (a) successful placement of probe; (b) needle has resurfaced.

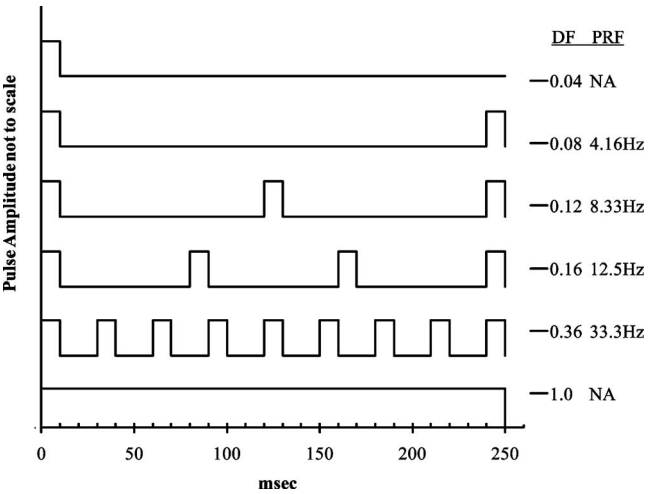

Fig. 2 TTL signal laser pulse sequences, with duty factors (DFs) and pulse repetition frequencies (PRFs) listed.

pigs was obtained from the University Institutional Animal Care and Use Committee. Tissue sample disposal procedures were approved by the Institutional Biosafety Committee (IBC) of the Research Integrity and Compliance Office.

Skin samples were excised from the rear flank of pigs within 24 h of animal euthanasia. Skin excision was performed in the Veterinary Medicine Anatomy Lab. After identifying a suitable area of skin free of injury or scars, with uniform pigmentation, the hair was removed with electric clippers set to the closest setting that would not scratch the skin. This left hair of approximately 1.5-mm length on the skin. Skin samples of approximately 100 cm^2 were taken with approximately 0.5 cm of fatty tissue thickness. The samples were maintained at 5 °C in airtight containers with 1 ml saline solution to maintain moisture. Skin samples were handled from the sides and edges to avoid any abrasion or tearing of the surfaces to be irradiated.

Under optical magnification, a 25-gauge, 5/8-in, hypodermic needle (Becton Dickenson, Franklin Lakes, New Jersey) was used to pierce the surface of the skin and was directed parallel to the skin surface. The HYP-0 thermocouple needle was immediately inserted through the 25-g needle until it extended 10 mm past the tip. This method proved to be the most reliable to insert the probe, as the 33-g needle construction of the thermocouple was too fragile to penetrate the skin by itself. The thermocouple insertion is shown in Fig. 1.

Insertion attempts were balanced between the goal of positioning the probe at shallow depth and the tendency to penetrate the delicate epidermal tissue from the inside [see Fig. 1(b)]. When this occurred, the needle was withdrawn from the hole and the process begun again 5 mm lateral to the ruptured hole site. The sample with the thermocouple inserted was then mounted on the optical translation stage using screws and rubber washers to clamp down a Petri dish containing the skin sample.

2.3 *Laser and Optics*

The pig skin was irradiated with a commercial 50-W Tm:YAG fiber laser (IPG Photonics, Oxford, Massachusetts), producing a 2.01-μm wavelength beam. The laser pulse sequences were created by two model 33120A 15-MHz digital wave form generators (Hewlett Packard, Englewood, Colorado) connected in series to control the duration and number of laser pulses, respectively. A single 10-ms laser pulse was created by setting the first wave form generator to deliver a single 50-Hz square-wave pulse, and offsetting the voltage by half the amplitude, thereby generating a TTL signal that served as a trigger for the laser control. The six pulse sequences were repetitions of the 10- ms single pulses as triggered by the second wave form generator, which was set to the desired PRF (see Fig. 2 for illustration of the multipulse sequence timing). In all sequences, individual 10-ms pulses were fired within a 250-ms period. The 50-W laser was adjusted in power to produce approximately equal total radiant exposures for each sequence.

The IR laser pulses were aligned to be colinear with a commercial HeNe laser (Model 05-LLR-811, Melles-Griot, Carlsbad, California) using a dual-axis adjustable gold mirror (Model PF20-03-M01, ThorLabs, Newton, New Jersey) with average reflectivity greater than 98% from 1 μm to 5 μm. This HeNe was selected in part for the low divergence of its beam at 1.7 mrad in the far field. The HeNe beam was essential to the laser operator for aiming the beam. The colinear beams were then directed into a custom optical articulating arm assembly (Oxid Corp., Farmington Hills, Michigan). This arm used seven articulating joints with gold mirrors to allow both the visible and IR beams to be directed to the measurement site safely. The laser and optics are diagrammed in Fig. 3.

The 2% of the IR beam reflected by the HeNe alignment mirror was measured and recorded for each exposure of the pig skin. The IR laser output from the articulating arm was calibrated to the split beam sample prior to each exposure session. A total of 21 exposures were simultaneously measured by both the sampling probe and another probe placed on the optical stage in place of the skin sample. The beam probes were PM10 air-cooled thermopile sensors (Coherent, Santa Clara, California) calibrated by the manufacturer with an uncertainty of ±1%. The sensors were read by an EPM2000 model meter (Coherent). The meter was also calibrated by the manufacturer with a stated resolution of ±0.03% of full-scale reading. The beam output and sampling data points covered laser settings from 30% to 100% power output and were fit to a straight line with correlation coefficient greater than 0.98 without forcing the intercept to zero. This provided a high

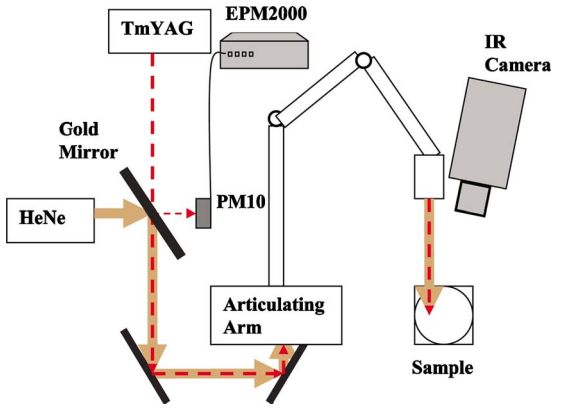

Fig. 3 Optics path: IR beam is dashed, red positioning beam is gray.

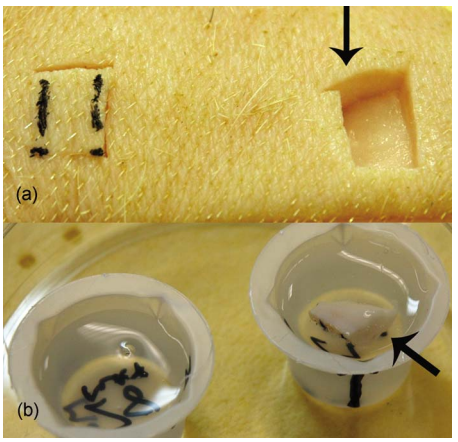

Fig. 4 Pig skin after exposure during preparation for freezing: (a) needle insertion marked with ink on left and sample cut out on right; (b) inked and cut sample in OCT solution in labeled freezing cup on right, and OCT for unexposed skin on left.

confidence in the calculated beam energy for each exposure.

The IR beam incident on the pig skin had a Gaussian shape with a 3.28 mm $1/e^2$ radius using a pinhole technique[66] in both directions. Beam diameter was measured in both directions on five occasions throughout the study, with a standard deviation of 0.33 mm between all results. Beam shape was confirmed to be uniform, circular in the lowest order mode, and aligned with the HeNe beam using Zap-It thermal paper (Kentek, Pittsfield, New Hampshire) prior to each measurement session. Exposures were made on the thermal paper prior to the beam entering the armature and after the beam exiting the arm at the level of the skin sample. The thermal paper impressions were then visually compared to previous sessions' marks to identify any changes. The thermal paper exposures were performed using a four-pulse sequence with the laser set to 50% power to produce reasonable beam patterns both entering and exiting the articulating arm with the same laser settings.

2.4 *Histology*

After the laser exposures were completed, the surface of the pig skin was marked with black ink parallel to the needle from the insertion point to the end of the probe. The HYP-O probe was then withdrawn from the sample and from the 25-g needle. Before the 25-g needle was withdrawn, a 3-cc syringe containing yellow tissue marking dye (Cancer Diagnostics, Inc., Birmingham, Michigan) was connected to the Leur-lock of the needle. As the 25-g needle was withdrawn from the skin, gentle pressure on the syringe injected the dye into the cavity evacuated by the needle. This prevented the cavity from collapsing on itself and rendered it clearly distinguishable under a microscope. The pressure on the syringe plunger was minimal, to prevent the dye from being forced into the surrounding tissue and expanding or rupturing the cavity. The sample was then cut down with 2-mm margins around the ink marks and submerged in the freezing solution, Tissue-Tek OCT (Sakura Fintek, Torrance, California), as shown in Fig. 4.

In order to freeze the sample in a known orientation, the skin was held in place with cotton thread sutured to the edges deep in the muscle layer of the sample. This was necessary to prevent sectioning geometry uncertainty. The sample container was marked with the needle direction and sample number. It was then frozen for 24 h at −80°C. The frozen sample was affixed to a ball joint holder with (OCT) solution and mounted in the microtome (Bright Instruments, Huntington UK), as shown in Fig. 5. The sample was aligned perpendicular to the knife edge and trimmed down until the black ink markings on the surface, indicating the needle insertion, were visible. As soon as the black ink was identified, sections of 15-μm thickness were cut and mounted on slides. Digital images were taken of the slides at 4× magnification on a BH2 microscope (Olympus, Center Valley, Pennsylvania), as shown in Fig. 6. Depths were measured on the images to the center of the dye-stained hole using Spot software version 4.09 (Digital Instruments, Inc., Sterling Heights, Michigan). Measurements from the four distal images showing the probe cavity were averaged with a maximum standard deviation of a sample being 0.065 mm at the 0.650-mm depth. The distance measurement function of the Spot software was calibrated for the 4× lens with a digital test pattern, Model USAF1951 (Edmund Optics, Barrington, New Jersey).

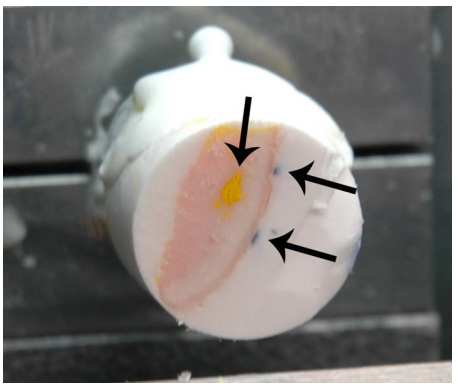

Fig. 5 Pig skin sample frozen in OCT mounted in the microtome. Notice the black ink marks visible on the surface (horizontal arrows) and the large yellow dye spot (vertical arrow) from excessive pressure on the syringe during needle withdrawal. (Yellow dye from successful injection yields inadequate contrast to identify in photographs.) (Color online only.)

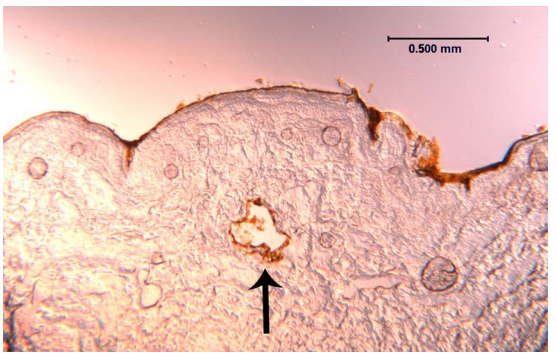

Fig. 6 Histology image of pigskin showing the dye-marked thermocouple probe hole (arrow) and the ink marked surface. (Ink appears brown in the two valleys on either side of the hole.) (Color online only.)

2.5 *Data Analysis*

Temperature for each exposure was measured simultaneously both at depth and on the surface. The relative temperature rise per exposure in $^{\circ}\mathrm{C\,mJ^{-1}\,mm^2}$ was calculated. In the case of the thermocouple temperature, baseline was taken as the first data point. The thermal camera was set to take 20 data points prior to the exposure for background subtraction.

The maximum temperature rise per exposure ($\Delta^{\circ}\mathrm{C\,mJ^{-1}\,mm^2}$) for each pulse sequence was examined with an analysis of variance (ANOVA) to determine whether any differences existed between the pulse sequences. The data were then compared with Fisher's least significant difference (LSD) procedure to find which sequences produced a different temperature rise at the 95% confidence level.

The measured temperatures were then compared to expected temperatures calculated with an adaptation of the Green's function solution to the tissue bioheat differential equation from Vyas and Rustgi [Eq. (3)].[40] As there was no blood flow in the pigskin samples, the first exponential term from the published solution is one and is dropped. The second exponential term from Vyas and Rustgi is also one for these central axis ($r=0$) temperatures, and is therefore omitted. For the multiple-pulse exposures, the calculated temperatures from the individual pulses were summed at the end of the pulse sequence. The Vyas solution was chosen over the Grossweiner et al.[39] or the Roider et al.[26] solutions, as it describes the temperature in both the depth and radial directions with time:

$$T(z,t) = \left[\frac{\mu_a E_o}{\pi\rho C}\frac{1}{(a^2+8Dt)}\right] \times[\exp(-\mu_a z+\mu_a^2 Dt)]\mathrm{erfc}\left(\frac{2D\mu_a t - z}{\sqrt{4Dt}}\right). \quad (3)$$

In Eq. (3), μ_a is the optical absorption coefficient for the tissue, E_o is the energy deposited, ρ is the tissue density, C is the specific heat capacity, a is the laser beam $1/e^2$ radius, D is the tissue thermal diffusivity, z is the depth in tissue, and t is the time. The literature provides a wide range of values for the thermal constants for skin tissue, as listed in Table 2. The constants used in this study were as follows: $\mu_a = 2.176\ \mathrm{mm^{-1}}$ (Ref. 32); $\rho = 0.00107\ \mathrm{g\,mm^{-3}}$ (Refs. 55 and 61); $C = 3.4\ \mathrm{J\,g^{-1}\,^{\circ}C^{-1}}$ (Ref. 55); $D = 0.12\ \mathrm{mm^2\,s^{-1}}$ (Refs. 40 and 60); and the beam radius $a = 3.2$ mm. These values were chosen because they fall near the middle of the range of published values and the diffusivity value was also used by Vyas and Rustgi.

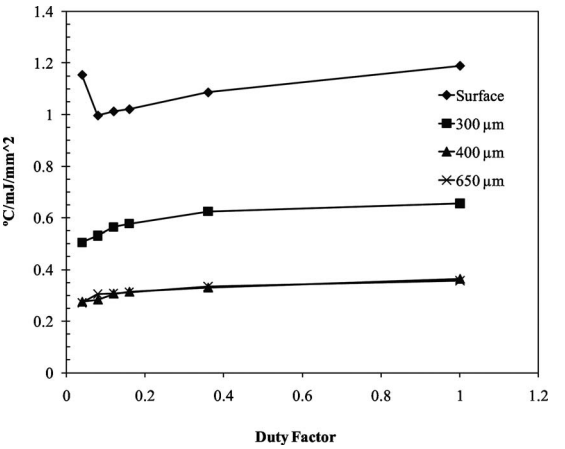

Fig. 7 Graph of measured temperature rise per exposure at four depths in pig skin versus duty factor of the pulse sequence.

3 Results

The temperature of pig skin was measured simultaneously on the surface and at depth during six different pulsing sequences of 2.0-μm laser exposure. Four measurements of each sequence on three different skin samples produced at least 12 data points for each sequence at depths of 300 μm, 400 μm, and 650 μm. The IR camera provided surface temperature readings during each irradiation. The measurements produced repeatable temperature increases per incident exposure with the maximum variance of a data group at $0.013\ ^{\circ}\mathrm{C\,mJ^{-1}\,mm^2}$ for the single-pulse (duty factor 0.04)

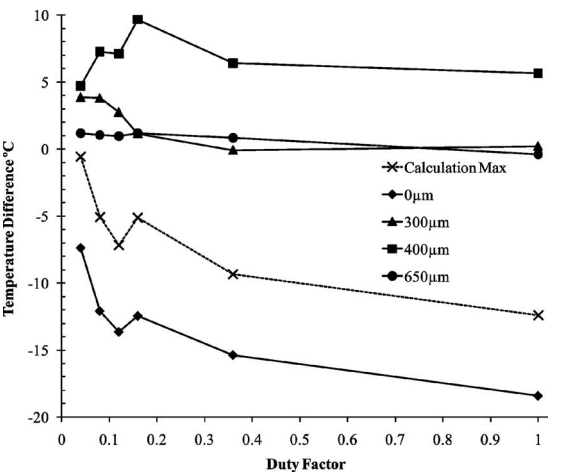

Fig. 8 Difference between calculated and measured temperature rise for exposures used in study. Calculation maximum temperature and calculated zero depth temperatures are compared to IR camera measurements, while temperatures at depth relate to thermocouple measurements. The depths of the calculated maximum temperatures are given in Fig. 9.

Table 5 ANOVA results.

Depth	*p*-value	S_w^2
Surface	1.47×10^{-23}	0.00874
300 μm	0.000914	0.00875
400 μm	0.000852	0.00290
650 μm	8.07×10^{-10}	0.00073

surface data. The depth of measurement was determined by histological examination of the irradiated skin with a maximum variance of 0.004 mm, attributed to the irregular surface of skin within a sample. The measurements were compared to expected temperatures calculated with an analytical expression.

3.1 *Temperature Rise per Exposure—Measured*

The temperature rise per H in °C mJ^{-1} mm^2 was measured at four depths in pig skin using six different laser pulse patterns. The measured results, shown in Fig. 7, reveal a different pattern on the surface at low duty factor compared to the measurements below the optical penetration depth. As the duty factor increases, the temperature rise per exposure levels off.

3.2 *Temperature Rise per Exposure—Calculated*

The difference between the temperatures calculated using the Vyas equation for the pulse sequences under consideration and the corresponding measured temperatures are shown in Fig. 8. Here, the surface temperature calculated was dramatically less than the measured temperature for all but the single-pulse sequence. Below the surface, the temperatures calculated from the model were higher than the measured results. The calculated temperatures at 0.4-mm depth were 5 to 10 degrees higher than measured. This corresponds to the measurements at 0.4 mm, being equivalent to the temperatures at 0.65 mm seen in Fig. 7. Calculated temperatures at 0.65-mm depth matched the measured temperatures reasonably well for all duty factors. The model results gave maximum temperatures at depths between 90 μm and 170 μm, as shown in Fig. 9.

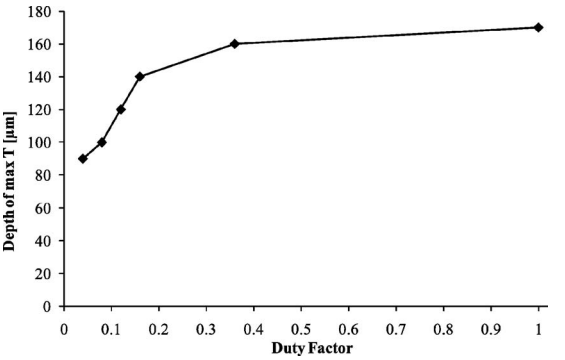

Fig. 9 Calculated skin depth of maximum temperature from exposure to TmYAG laser.

3.3 *Statistical Analysis*

Comparing the measured temperatures per exposure between the different pulse sequences, the ANOVA showed that there were significant differences between pulse sequences at each depth at the 95% confidence level. A summary of the *p*-values and variance within each group are given in Table 5.

The LSD procedure performed for each depth showed that the differences were between the low duty factor sequences and the high duty factor sequences. The relations between sequences are given in Tables 6–9 for depths from surface to 650 μm. Within each depth's table, the italicized results indicate that the two sequences produced insignificantly different temperature rise per unit exposure to 2.0-μm laser irradiation. The bold values were found to be statistically different from each other.

The different pulse sequences were found to produce statistically different temperature rise per total exposure at all four depths, with *p*-values less than 0.001 from ANOVA results. At all depths, the two-pulse, three-pulse, and four-pulse sequences were equivalent. The 300-μm and 400-μm depths produced temperatures that were not significantly different from the temperature rise produced between adjoining sequences.

4 Discussion

The temperature rise per exposure on the surface was found to follow a different trend at low duty factor (single pulse) than

Table 6 Significant difference in temperature per exposure at surface (significant differences in bold; differences less than Fisher's LSD, 0.031, in italics).

Pulse sequence	1 pulse	2 pulse	3 pulse	4 pulse	9 pulse	25 (CW)
1 pulse	—	**–0.16**	**–0.14**	–0.13	**–0.07**	**0.04**
2 pulse	**0.16**	—	*0.02*	*0.02*	**0.09**	**0.19**
3 pulse	**0.14**	*–0.02*	—	*0.01*	**0.07**	**0.18**
4 pulse	**0.13**	*–0.02*	*–0.01*	—	**0.07**	**0.17**
9 pulse	**0.07**	**–0.09**	**–0.07**	**–0.07**	—	**0.10**
25 (CW)	**–0.04**	**–0.19**	**–0.18**	**–0.17**	**–0.10**	—

Table 7 Significant difference in temperature per exposure at 0.30 mm (significant differences in bold; differences less than Fisher's LSD, 0.054, in italics).

Pulse sequence	1 pulse	2 pulse	3 pulse	4 pulse	9 pulse	25 (CW)
1 pulse	—	*0.03*	**0.06**	**0.07**	**0.12**	**0.15**
2 pulse	*−0.03*	—	*0.03*	*0.05*	**0.09**	**0.12**
3 pulse	**−0.06**	*−0.03*	—	*0.01*	**0.06**	**0.09**
4 pulse	**−0.07**	*−0.05*	*−0.01*	—	*0.05*	**0.08**
9 pulse	**−0.12**	**−0.09**	**−0.06**	*−0.05*	—	*0.03*
25 (CW)	**−0.15**	**−0.12**	**−0.09**	**−0.08**	*−0.03*	—

the temperatures measured at depths below the surface. The measurements below the surface represent direct heating as well as heat flow from tissue above. The increase in temperature appears to rise as the duty factor increases for depths below the surface. In contrast, from the IR camera measurements, this trend does not hold for the single-pulse (low duty factor) sequence on the surface.

However, as seen in Fig. 8, the calculated temperatures using the Vyas model demonstrate that the model was very good at predicting temperature for 650-μm depth for all duty factors from one pulse up to CW. The model's predicted temperatures were 5° to 10°C high for the 400-μm depth for all duty factors, with the largest difference at the medium duty factor of 0.16. The linear superposition of multiple pulses exaggerated the model's difference from measured temperature. At a 300-μm depth in skin, the calculations were within 1° for duty factors of 0.16 and higher, but increasingly diverged to 7°C from measurements at lower duty factors. This was unexpected from this model, which was originally validated with microsecond pulse widths.

The Vyas model did not predict surface temperatures well. At shallow depths, either exact skin surface (z=0 μm) or at the depths of calculated maximum temperatures, the model underestimated temperature rise. The Vyas model was best at predicting temperatures for the smallest duty factor (0.04). The predicted temperatures fell significantly below measured temperatures by approximately 5 to 7°C for the middle duty factors (0.08 to 0.16). As the duty factor increased to 0.36 and above, the model underestimated the temperatures by 10°C. At the calculated air–skin interface (z=0 μm), the predicted temperatures were 6°C lower, while following the same pattern with duty factor. The agreement of measurements to calculated temperatures near, but not at, the air–skin interface indicated that the IR camera's microbolometer is responding to IR emitted by a region below the skin surface. The Vyas model produced maximum temperatures at increasing depths between 90 μm and 170 μm, as seen in Fig. 9. The disagreement between the model and the measurements becomes larger as the maximum temperature occurs deeper in the skin. This discrepancy is most significant because it occurs in the region of the basal layer of the epidermis in human skin.

The analysis of measured temperature rise per exposure between pulse sequences of different duty factors showed a significant difference between some of the sequences, but not the same ones at different depths. For the surface and 650-μm depths of Tables 4 and 7, the measured rise per exposure was found to be statistically different between any combination two sequences, including one with a duty factor of 0.04 or above 0.36. The single-pulse, the nine-pulse, and the CW irradiations were different from any other sequence. At 300-μm and 400-μm depths in Tables 5 and 6, the single-pulse sequence was equivalent to the double-pulse sequence, but different from all higher duty factors. The 300-μm and

Table 8 Significant difference in temperature per exposure at 0.40 mm (significant differences in bold; differences less than Fisher's LSD, 0.031, in italics).

Pulse squence	1 pulse	2 pulse	3 pulse	4 pulse	9 pulse	25 (CW)
1 pulse	—	*0.01*	**0.03**	**0.04**	**0.05**	**0.09**
2 pulse	*−0.01*	—	*0.02*	*0.03*	**0.05**	**0.08**
3 pulse	**−0.03**	*−0.02*	—	*0.01*	*0.02*	**0.06**
4 pulse	**−0.04**	*−0.03*	*−0.01*	—	*0.02*	**0.05**
9 pulse	**−0.05**	**−0.05**	*−0.02*	*−0.02*	—	**0.03**
25 (CW)	**−0.09**	**−0.08**	**−0.06**	**−0.05**	**−0.03**	—

Table 9 Significant difference in temperature per exposure at 0.65 mm (significant differences in bold; differences less than Fisher's LSD, 0.015, in italics).

Pulse sequence	1 pulse	2 pulse	3 pulse	4 pulse	9 pulse	25 (CW)
1 pulse	—	**0.03**	**0.04**	**0.04**	**0.06**	**0.09**
2 pulse	**–0.03**	—	*0.00*	*0.01*	**0.03**	**0.05**
3 pulse	**–0.04**	*0.00*	—	*0.00*	**0.03**	**0.05**
4 pulse	**–0.04**	*–0.01*	*0.00*	—	**0.02**	**0.04**
9 pulse	**–0.06**	**–0.03**	**–0.03**	**–0.02**	—	**0.02**
25 (CW)	**–0.09**	**–0.05**	**–0.05**	**–0.04**	**–0.02**	—

400-μm depths were unique in the temperature rise per exposure relations between sequences of higher duty factor. At 300-μm depth, a sequence with duty factor of 0.36 was equivalent to both a CW irradiation and a pulse sequence with duty factor of 0.16. At 400-μm depth, a sequence with duty factor of 0.36 was different from the CW irradiation but equivalent to both a 0.16 and 0.12 duty factor sequence. Therefore, while there were several combinations of pulse sequence, duty factors producing equivalent temperature rise per radiant energy, only the nine-pulse sequence with duty factor 0.36 heated the tissue the same as a CW beam at 300 μm. At all depths then, the pulsed beams produced lower temperatures per radiant exposure than did the CW beam for equivalent energy input.

The maximum temperatures measured at the 400-μm and 650-μm depths were virtually the same for all duty factors, all within one standard deviation. By a simple Beer's law calculation, there is at least an order of magnitude difference in incident beam energy at these two depths. Chen's attenuation coefficient of 21.76 cm^{-1} gives the closest beam intensities at depths of 400 μm and 650 μm from among the various attenuation coefficient values from Table 1. This attenuation coefficient used in Vyas's model also predicted temperatures closest to the measurements. Therefore, there appears to be rapid heat transfer in the axial direction to bring the deeper measurements to the same maximum temperature. However, the significant differences between pulse sequences of 0.36 duty factor at 650 μm that are not found at 400 μm indicate that the heat flows fast enough to distinguish each separate pulse at duty factors between 0.04 and 0.36. The differences in temperature normalized to radiant energy indicate that the assumption of linear superposition of successive pulses does not represent the thermal dynamics of pulsed irradiation of skin for pulse sequences with duty factors between 0.04 and 0.36 at depths from the surface to 650 μm, roughly the middle of the dermis. The ANSI Z136.1 limit of radiant exposure for 250-ms pulse sequences of 2.0-μm IR is $MPE = 0.56 \times 0.250^{00.25} = 0.396$ J cm^{-2}, which is roughly 10 times less than the maximum exposure of 3.17 J cm^{-2} delivered in this study. It is worth noting that while the exposures delivered in this study were very close to the ED_{50} levels of Chen et al.[5] for *in vivo* pig skin (3.6 J cm^{-2} and 2.9 J cm^{-2} for beams of radii of 2.4 mm and 4.8 mm, respectively), no reddening of the *ex vivo* skin was observed. Furthermore, the maximum absolute temperature increase recorded was 36.2 °C from the IR camera surface measurement of an exposure sequence with 0.16 duty factor. The maximum temperature increase for any one exposure beneath the surface was 20.7 °C above background for a 0.16 duty factor sequence at 300-μm depth. This increase is over twice Moncrief's "brief" temperature tolerated by skin, yet even with no vascular heat removal, no damage was observed visually or on the histology slides. Therefore, the ANSI Z136.1 limitations for skin exposure are shown to be inherently conservative, as they do not apply the Rule 3 correction factor based on number of pulses to skin. However, a correction factor based on pulse sequence duty factor may be appropriate in this region of the far infrared.

The differences in temperature rise per unit exposure between the pulse sequences can be explained by significant heat conduction during the pulses. Therefore, the common assumption of thermal confinement may need to be experimentally verified.

Acknowledgments

The views expressed in this article are those of the authors and do not reflect the official policy or position of the U. S. Air Force, The Department of Defense, or the U.S. Government. We want to acknowledge and thank Dr. Robert E. Lee, Antonio Serpa, and Aimee Oke for their generous support and expertise.

References

1. T. H. Maiman, "Stimulated optical radiation in ruby," *Nature* **187**, 494–495 (1960).
2. L. Goldman, D. J. Blaney, D. J. Kindel, and E. K. Franke, "Effect of the laser beam on the skin," *J. Invest. Dermatol.* **40**, 121–122 (1963).
3. C. H. Powell and L. Goldman, "Recommendations of the laser safety conference," *Arch. Environ. Health* **18**, 448–452 (1969).
4. American National Standards Institute, American National Standard for Safe Use of Lasers, ANSI Z136-1-2007 (2007).

5. B. Chen, D. O'Dell, S. Thomsen, B. Rockwell, and A. Welch, "Porcine skin ED50 damage thresholds for 2000-nm laser irradiation," *Lasers Surg. Med.* **37**, 373–381 (2005).
6. A. R. Moritz and F. C. Henriques, "Studies of thermal injury: the relative importance of time and surface temperature in the causation of cutaneous burns," *Am. J. Pathol.* **23**(5), 695–720 (1947).
7. J. A. Moncrief, "The body's response to heat," Chap. 3 in *Burns, A Team Approach*, C. P. Artz, J. A. Moncrief, and B. A. Pruitt, Eds., Saunders, Philadelphia (1979).
8. E. H. Leach, R. A. Peters, and R. J. Rossiter, "Experimental thermal burns, especially the moderate temperature burns," *Q. J. Exp. Physiol. Cogn Med. Sci.* **32**, 67–86 (1943).
9. R. J. Rockwell, "Research on human skin laser damage thresholds," Report DERM-LL-74-1003 to USAF School of Aerospace Medicine (1974).
10. R. Hibst and R. Kaufmann, "Effects of laser parameters on pulsed Er-YAG laser skin ablation," *Lasers Med. Sci.* **6**, 391–397 (1991).
11. M. Leandri, M. Saturno, L. Spadaveccia, G. D. Iannetti, G. Cruccu, and A. Truini, "Measurement of skin temperature after infrared laser stimulation," *Clin. Neurophysiol.* **36**, 207–218 (2006).
12. B. Bromm and R. D. Treede, "CO_2 laser radiant heat pulses activate C nociceptors in man," *Pfluegers Arch.* **399**, 155–156 (1983).
13. Y. Ito, R. Kennan, E. Watanabe, and H. Koizumi, "Assessment of heating effects in skin during continuous wave near-infrared spectroscopy," *J. Biomed. Opt.* **5**(4), 383–390 (2000).
14. J. Howard, P. Arango, J. Ossoff, R. Ossoff, and L. Reinisch, "Healing of laser incisions in rat dermis: comparison of carbon dioxide laser under manual and computer control and the scalpel," *Lasers Surg. Med.* **20**, 90–96 (1997).
15. C. P. Cain, K. J. Schuster, J. J. Zohner, K. L. Stockton, D. J. Stolarski, R. J. Thomas, B. A. Rockwell, and W. P. Roach, "Visible lesion thresholds with pulse duration, spot size dependency, and model predictions for 1.54-μm, near-infrared laser pulses penetrating porcine skin," *J. Biomed. Opt.* **11**(2), 024001 (2006).
16. A. T. Jain, M. S. Blumendranz, Y. Paulus, M. W. Wiltberger, D. E. Anderson, P. Huie, and D. Palanker, "Effect of pulse duration on size and character of the lesion in retinal photocoagulation," *Arch. Opthal.* **126**(1), 78–85 (2008).
17. J. M. Garden, O. T. Tan, R. Kershmann, J. Boll, H. Furumoto, R. R. Anderson, and J. A. Parrish, "Effect of dye laser pulse duration on selective cutaneous vascular injury," *J. Invest. Dermatol.* **85**(5), 653–657 (1986).
18. K. A. Khatri, "The effects of variable pulse width of Er:YAG laser on facial skin," *Dermatol. Surg.* **27**(4), 332–334 (2001).
19. E. V. Ross, J. R. McKinlay, F. P. Sajben, C. H. Miller, D. J. Barnette, K. J. Meehan, N. P. Chieng, M. J. Deavers, and B. D. Zelickson, "Use of a novel erbium laser in a Yucatan minipig: a study of residual thermal damage, ablation, and wound healing as a function of pulse duration," *Lasers Surg. Med.* **30**, 93–100 (2002).
20. R. M. Adrian, "Pulsed carbon dioxide and long pulse 10-ms erbium-YAG laser resurfacing: a comparative clinical and histologic study," *J. Cut. Laser Ther.* **1**, 197–202 (1999).
21. E. D. Jansen, T. H. Le, and A. J. Welch, "Excimer, Ho:YAG, and Q-switched Ho:YAG ablation of aorta," *Appl. Opt.* **32**(4), 526–534 (1993).
22. M. A. Trelles, S. Mordon, V. Benitez, and J. L. Levy, "Er:YAG laser resurfacing using combined ablation and coagulation modes," *Dermatol. Surg.* **27**(8), 727–734 (2001).
23. R. E. Fitzpatrick, S. R. Smith, and S. Sriprachya-Anunt, "Depth of vaporization and the effect of pulse stacking with a high-energy pulsed carbon dioxide laser," *J. Am. Acad. Dermatol.* **40**(4), 615–622 (1999).
24. A. D. Zweig and H. P. Weber, "Mechanical and thermal parameters in pulsed laser cutting of tissue," *IEEE J. Quantum Electron.* **23**(10), 1787–1793 (1987).
25. S. L. Jacques and S. A. Prahl, "Modeling optical and thermal distributions in tissue during laser irradiation," *Lasers Surg. Med.* **6**, 494–503 (1987).
26. J. Roider, F. Hillenkamp, T. Flotte, and R. Birngruber, "Microphotocoagulation: selective effects of repetitive short laser pulses," *Proc. Natl. Acad. Sci. U.S.A.* **90**, 8643–8647 (1993).
27. N. A. Peppers, A. Vassiliadis, K. G. Dedrick, H. Chang, R. R. Peabody, H. Rose, and H. C. Zweng, "Corneal damage thresholds for CO_2 laser radiation," *Appl. Opt.* **8**(2), 377–381 (1969).
28. P. Parsa, S. L. Jacques, and N. S. Nishioka, "Optical properties of rat liver between 350 and 2200 nm," *Appl. Opt.* **28**(12), 2325–2330 (1989).
29. R. Birngruber, F. Hillenkamp, and V. P. Gabel, "Theoretical investigations of laser thermal retinal injury," *Health Phys.* **48**(6), 781–796 (1985).
30. S. L. Jacques, "Role of tissue optics and pulse duration on tissue effects during high-power laser irradiation," *Appl. Opt.* **32**(13), 2447–2454 (1993).
31. J.-P. Ritz, A. Roggan, C. Isbert, G. Muller, H. J. Buhr, and C.-T. Germer, "Optical properties of native and coagulated porcine liver tissue between 400 and 2400 nm," *Lasers Surg. Med.* **29**, 205–212 (2001).
32. B. Chen, S. L. Thomsen, R. J. Thomas, and A. J. Welch, "Modeling thermal damage in skin from 2000-nm laser irradiation," *J. Biomed. Opt.* **11**(6), 064028 (2006).
33. J. H. Torres, M. Motamedi, J. A. Pearce, and A. J. Welch, "Experimental evaluation of mathematical models for predicting the response of tissue to laser irradiation," *Appl. Opt.* **32**(4), 597–606 (1993).
34. A. N. Bashkatov, E. A. Genina, V. I. Kochuvey, and V. V. Tuchin, "Optical properties of human skin, subcutaneous and mucous tissues in the wavelength range from 400 to 2000 nm," *J. Phys. D* **38**, 2543–2555 (2005).
35. T. L. Troy and S. N. Thennadil, "Optical properties of human skin in the near-infrared wavelength range of 1000 to 2200 nm," *J. Biomed. Opt.* **6**(2), 167–176 (2001).
36. R. R. Anderson and J. A. Parrish, "The optics of human skin," *J. Invest. Dermatol.* **77**, 13–19 (1981).
37. A. Vogel and V. Venugopalan, "Mechanisms of pulsed laser ablation of biological tissue," *Chem. Rev.* **103**, 577–644 (2003).
38. N. P. Furzikov, "Different lasers for angioplasty: thermooptical comparison," *IEEE J. Quantum Electron.* **23**(10), 1751–1755 (1987).
39. L. I. Grossweiner, A. M. Al-Karmi, P. W. Johnson, and K. R. Brader, "Modeling of tissue heating with a pulsed Nd:YAG laser," *Lasers Surg. Med.* **10**, 295–302 (1990).
40. R. Vyas and M. L. Rustgi, "Green's function solution to the tissue bioheat equation," *Med. Phys.* **19**(5), 1319–1323 (1992).
41. C. P. Cain and A. J. Welch, "Measured and predicted laser-induced temperature rises in the rabbit fundus," *Invest. Ophthalmol.* **13**(1), 60–70 (1974).
42. D. Schaaf, T. Eurrel, and T. Johnson, "Cultured human keratinocytes for optical transmission measurement," *J. Biophotonics* **3**, 161–168 (2010).
43. F. Xu, T. J. Lu, and K. A. Seffen, "Biothermomechanical behavior of skin tissue," *Acta Mech. Sin.* **24**, 1–23 (2008).
44. T. J. Pfefer, D. J. Smithies, T. E. Milner, M. J. van Gemert, J. S. Nelson, and A. J. Welch, "Bioheat transfer analysis of cryogen spray cooling during laser treatment of port wine stains," *Lasers Surg. Med.* **26**, 145–157 (2000).
45. T. R. Gowrishankar, D. A. Stewart, G. T. Martin, and J. C. Weaver, "Transport lattice models of heat transport in skin with apatially heterogeneous, temperature-dependent perfusion," *Biomed. Eng. Online* **3**, 42 (2004).
46. A. M. Stoll, "Thermal properties of human skin related to nondestructive measurement of epidermal thickness," *J. Invest. Dermatol.* **69**(3), 328–332 (1977).
47. M. L. Cohen, "Measurement of the thermal properties of human skin," *J. Invest. Dermatol.* **69**(3), 333–338 (1977).
48. H. F. Bowman, E. G. Cravalho, and M. Woods, "Theory, measurement, and application of thermal properties of biomaterials," *Annu. Rev. Biophys. Bioeng.* **4**, 43–80 (1975).
49. B. Anvari, T. E. Milner, S. Tanenbaum, and J. S. Nelson, "A comparative study of human skin thermal response to sapphire contact and cryogen spray cooling," *IEEE Trans. Biomed. Eng.* **45**, 934–941 (1998).
50. Z.-S. Deng and J. Liu, "Analytical study on bioheat transfer problems with spatial or transient heating on skin surface or inside biological bodies," *J. Biomech. Eng.* **124**, 638–649 (2002).
51. O. S. Khalil, S. Yeh, M. G. Lowery, X. Wu, C. F. Hanna, S. Kantor, T.-W. Jeng, J. S. Kangar, R. A. Bolt, and F. F. de Mul, "Temperature modulation of the visible and near-infrared absorption and scattering coefficients of human skin," *J. Biomed. Opt.* **8**(2), 191–205 (2003).
52. J. A. Parrish, R. R. Anderson, T. Harris, B. Paul, and G. F. Murphy, "Selective thermal effects with pulsed irradiation from lasers: from organ to organelle," *J. Invest. Dermatol.* **80**(6), 75s–80s (1983).

53. B. Choi, J. A. Pearce, and A. J. Welch, "Modeling infrared temperature measurements: implications for laser irradiation and cryogen cooling studies," *Phys. Med. Biol.* **45**, 541–557 (2000).
54. M. K. Loze and C. D. Wright, "Temperature distributions in laser-heated biological tissue with application to birthmark removal," *J. Biomed. Opt.* **6**(1), 74–85 (2001).
55. J. J. Crochet, S. C. Gnyawali, Y. Chen, E. C. Lemley, L. V. Wang, and W. R. Chen, "Temperature distribution in selective laser-tissue interaction," *J. Biomed. Opt.* **11**(3), 034031 (2006).
56. V. Tuchin, *Tissue Optics*, SPIE Press, Bellingham, WA (2007).
57. J. C. Chato, "Selected thermophysical properties of biological materials," in *Heat Transfer in Medicine and Biology*, A. Shitzer and R. C. Eberhart, Eds., pp. 413–418, Plenum Press, New York (1985).
58. M. Lipkin and J. D. Hardy, "Measurement of some thermal properties of human tissues," *J. Appl. Physiol.* **7**(2), 212–217 (1954).
59. J. C. Chato, "Thermal properties of tissues," in *Handbook of Bioengineering*, R. Skalak and S. Chien, Eds., pp. 9.1–9.13, McGraw-Hill, New York (1987).
60. L. O. Svaasand, T. Boerslid, and M. Oeveraasen, "Thermal and optical properties of living tissue: application to laser-induced hyperthermia," *Lasers Surg. Med.* **5**, 589–602 (1985).
61. T. S. Sandhu, "Measurement of blood flow using temperature decay: effect of thermal conditions," *Int. J. Radiat. Oncol., Biol., Phys.* **12**(3), 373–378 (1986).
62. F. Manns, P. J. Milne, X. Gonzalez-Cirre, D. B. Denham, J. M. Parel, and D. S. Robinson, "*In situ* temperature measurements with thermocouple probes during laser interstitial thermotherapy (LITT)," *Lasers Surg. Med.* **23**, 94–103 (1998).
63. C. P. Cain and A. J. Welch, "Thin-film temperature sensors for biological measurements," *IEEE Trans. Biomed. Eng.* **21**(5), 421–423 (1974).
64. J. W. Valvano and J. Pearce, "Temperature measurements," in *Optical–Thermal Response of Laser Irradiated Tissue*, A. J. Welch and M. J. C. vanGemert, Eds., p. 518, Plenum Press, New York (1995).
65. G. M. Hale and M. R. Querry, "Optical constants of water in the 200-nm to 200-micron wavelength region," *Appl. Opt.* **12**(3), 555–563 (1973).
66. P. J. Shayler, "Laser beam distribution in the focal region," *Appl. Opt.* **17**(17), 2673–2674 (1978).